Commun. Comput. Phys.
doi: 10.4208/cicp.231209.060111s

Vol. **11**, No. 2, pp. 610-628
February 2012

Complete Radiation Boundary Conditions for Convective Waves

Thomas Hagstrom[1,*], Eliane Bécache[2], Dan Givoli[3] and Kurt Stein[1]

[1] *Dept. of Mathematics, Southern Methodist University, Dallas, TX 75275, USA.*
[2] *Propagation des Ondes, Etude Mathématique et Simulation (POEMS), INRIA, Domaine de Voluceau-Rocquencourt, BP 105, 78153 Le Chesnay Cedex, France.*
[3] *Dept. of Aerospace Engineering, Technion, Haifa 32000, Israel.*

Received 23 December 2009; Accepted (in revised version) 6 January 2011

Available online 24 October 2011

Abstract. Local approximate radiation boundary conditions of optimal efficiency for the convective wave equation and the linearized Euler equations in waveguide geometry are formulated, analyzed, and tested. The results extend and improve for the convective case the general formulation of high-order local radiation boundary condition sequences for anisotropic scalar equations developed in [4].

AMS subject classifications: 65M12, 35L50, 35C15

Key words: Radiation boundary conditions, convective waves.

1 Introduction

The problem of imposing accurate and efficient radiation boundary conditions at nonphysical boundaries is central in the numerical analysis of wave propagation problems. For isotropic systems, recent results [14] provide local radiation boundary condition sequences which guarantee any desired accuracy using a minimal number of terms; precisely the complexity of the procedure scales as the logarithm of the error tolerance multiplied by the logarithm of the dimensionless parameter cT/δ where T is the simulation time, c is the wavespeed, and δ is the minimal separation between wave sources and the boundary. The goal of this paper is to extend these results to convective waves.

Low order local radiation boundary conditions for convective waves have been used for at least thirty years [5,16]. The first application of high-order conditions we know of,

*Corresponding author. *Email addresses:* thagstrom@smu.edu (T. Hagstrom), eliane.becache@inria.fr (E. Bécache), givolid@aerodyne.technion.ac.il (D. Givoli), kcstein@smu.edu (K. Stein)

however, came much later [13]. As advocated here, the implementation is based on auxiliary functions. The details of our current approach for general anisotropic scalar wave equations are given in [4]. What is new in this work is the combination of the general formulation in [4] with the optimal complete radiation boundary condition parameters derived in [14], the presentation of numerical experiments for convective problems, and the generalization of the construction to the linearized Euler equations. Here one must deal with the presence of vortical modes, which requires small changes to the boundary condition formulation.

We note that other accurate methods do exist for convective waves. Exact nonlocal conditions have been implemented for the linearized Euler equations in [1, 2, 10]; these are certainly accurate, but more costly and less flexible than the approach suggested here. Another approach is based on the so-called perfectly matched layer (PML). Although original formulations of PML for the linearized Euler equations were unstable [3], it was soon discovered how they could be stabilized [6,9,15]. As mentioned in [4], our boundary condition formulation can be interpreted as a nonstandard semidiscretized PML. However, for long time computations it is more efficient than the standard approach, as then the layer thickness must grow like $\sqrt{T}$. See, for example, the exact error analysis given by Diaz and Joly [7]. In any case, our method has the advantage of providing a parametrization with any prescribed accuracy without the need to tune ad hoc absorption or grid stretching profiles.

2 The convective wave equation

We first consider the equation

$$\left(\frac{\partial}{\partial t}+V_x\frac{\partial}{\partial x}\right)^2 u=c^2\nabla^2 u+f, \tag{2.1}$$

where, for definiteness, we assume a waveguide geometry

$$(x,y)\in\mathbb{R}\times\Omega,\ \ \alpha\frac{\partial u}{\partial n}+\beta u=0,\ \ y\in\partial\Omega, \tag{2.2}$$

a subsonic, rightmoving flow

$$0<M_x\equiv\frac{V_x}{c}<1, \tag{2.3}$$

and data, $u(x,y,0)$, $\frac{\partial u}{\partial t}(x,y,0)$, $f(x,y,t)$ supported in $(-L,L)\times\Omega$. Here $\Omega\subset\mathbb{R}^d$ in general, though our numerical experiments will be confined to $d=1$ and $\Omega=(-1,1)$. Also we assume that c, V_x and, therefore, M_x are constant. Our goal is to construct and test accurate, efficient radiation boundary conditions at $x_R=\pm(L+\delta)$ for δ small. A general theory of high-order radiation conditions for anisotropic and convective wave equations is developed in [4]. Here we combine that theory with the optimal parametrizations of [14], which we call complete radiation boundary conditions (CRBCs).

2.1 Construction and analysis of the boundary conditions

Solutions of (2.1)-(2.2) in the tails, $|x|>L$, can be written down using separation of variables. Precisely, we apply a Laplace transformation in time (dual variable s) and expand using the eigenvectors of the Laplacian in Ω,

$$\nabla_y^2\psi_k=-\eta_k^2\psi_k,\ \ y\in\Omega, \tag{2.4}$$

$$\alpha\frac{\partial\psi_k}{\partial n}+\beta\psi_k=0,\ \ y\in\partial\Omega. \tag{2.5}$$

As discussed in [4], we admit only outgoing waves in the tails as determined by their group velocity. Then

$$u=\sum_k\hat{u}_{k,+}(s)e^{\lambda_{k,+}x}\psi_k(y),\quad x<-L, \tag{2.6}$$

$$u=\sum_k\hat{u}_{k,-}(s)e^{\lambda_{k,-}x}\psi_k(y),\quad x>L, \tag{2.7}$$

where

$$\lambda_{k,\pm}=\frac{\bar{s}M_x\pm\gamma_k}{1-M_x^2}, \tag{2.8}$$

$$\gamma_k=\left(\bar{s}^2+(1-M_x^2)\eta_k^2\right)^{\frac{1}{2}}, \tag{2.9}$$

$\bar{s}=s/c$, and the branch of the root is such that $\Re\gamma_k>0$ when $\Re\bar{s}>0$.

Denoting by $\langle\cdot,\cdot\rangle$ the L^2-inner-product on Ω we derive from these expressions the exact boundary conditions

$$\left\langle\psi_k,\frac{\partial u}{\partial x}\right\rangle-\lambda_{k,+}\langle\psi_k,u\rangle=0,\qquad x=-(L+\delta), \tag{2.10}$$

$$\left\langle\psi_k,\frac{\partial u}{\partial x}\right\rangle-\lambda_{k,-}\langle\psi_k,u\rangle=0,\qquad x=L+\delta. \tag{2.11}$$

Approximate boundary conditions follow, ultimately, by rational approximations to the functions $\lambda_{k,\pm}$, or more directly to γ_k. (In the following u will denote the solutions obtained with the approximate boundary conditions.) In [4] we focus on approximants which are exact for some finite set of propagating plane waves,

$$\gamma_k\approx\cos\phi_j\bar{s},\qquad j=0,\cdots,P-1. \tag{2.12}$$

Here, instead, we match the complete wave expansion discussed in [14]. These are based on the observation that along a contour $\Re\bar{s}=1/(cT)$

$$\gamma_k=\cos\phi\bar{s}+\frac{\sin^2\phi}{cT\cos\phi},\qquad \phi\in\left[0,\frac{\pi}{2}\right). \tag{2.13}$$

Here T is a time scale over which we want to ensure accuracy; in practice we take it to be the simulation time.

2.1.1 Inflow boundary

In [4] an auxiliary variable formulation of the approximate boundary conditions is built directly for second order systems. However, it seems difficult to repeat that construction if approximations based on (2.13) are to be used. Therefore we generalize our technique, focusing on first order formulations. We can write (2.1) in $x<-L$ as a first order system for $q^T=(u\ \ v^T)$, where v is a new unknown. We emphasize that the new variable is only used at the boundary; (2.1) is solved throughout the interior. The equivalent first order system we consider is

$$\frac{1+M_x}{c}\frac{\partial u}{\partial t}-\left(1-M_x^2\right)\frac{\partial u}{\partial x}=(1+M_x)\nabla_y\cdot v, \tag{2.14}$$

$$\frac{1-M_x}{c}\frac{\partial v}{\partial t}+\left(1-M_x^2\right)\frac{\partial v}{\partial x}=(1-M_x)\nabla_y u. \tag{2.15}$$

Solving (2.14)-(2.15) for x-derivatives we obtain

$$\left(1-M_x^2\right)\frac{\partial q}{\partial x}=\mathcal{L}_I(\partial/\partial t,\nabla_y)q. \tag{2.16}$$

Noting that $\bar{s}\pm\gamma_k$ are eigenvalues of $\mathcal{L}_I$ (combined with boundary conditions), we introduce angles ϕ_j, $j=0,\cdots,2P-1$ and formally write down recursions for a sequence of auxiliary functions, $q_j^T=(u_j\ \ v_j^T)$, $j=0,\cdots,P$, starting from $q_0\equiv q$. Note that the auxiliary variables satisfy the same boundary conditions as q on $\partial\Omega$. At $x=-(L+\delta)$ we then have

$$\begin{aligned}&\mathcal{L}_I q_j-\frac{M_x+\cos\phi_{2j}}{c}\frac{\partial q_j}{\partial t}-\frac{\sin^2\phi_{2j}}{cT\cos\phi_{2j}}q_j\\ &=\mathcal{L}_I q_{j+1}-\frac{M_x-\cos\phi_{2j+1}}{c}\frac{\partial q_{j+1}}{\partial t}+\frac{\sin^2\phi_{2j+1}}{cT\cos\phi_{2j+1}}q_{j+1}.\end{aligned} \tag{2.17}$$

The recursion (2.17) may be motivated by performing a Laplace transform in time and appealing to (2.13). Expanding $\hat{q}_j$ in the eigenvectors of $\mathcal{L}_I$ we deduce that for outgoing waves with

$$\gamma_k=\cos\phi_{2j}\bar{s}+\frac{\sin^2\phi_{2j}}{cT\cos\phi_{2j}}$$

or incoming waves with

$$\gamma_k=\cos\phi_{2j+1}\bar{s}+\frac{\sin^2\phi_{2j+1}}{cT\cos\phi_{2j+1}}$$

the recursion terminates. This will be made clear by our analysis of the reflection coefficient presented in the case of the linearized Euler equations.

In terms of the first order hyperbolic system (2.14)-(2.15), u is a left-moving characteristic variable while v is right-moving. Writing out (2.17) we have

$$\begin{aligned}(1+\cos\phi_{2j+1})\frac{\partial u_{j+1}}{\partial t} &= (1-\cos\phi_{2j})\frac{\partial u_j}{\partial t} - \frac{\sin^2\phi_{2j}}{T\cos\phi_{2j}}u_j - \frac{\sin^2\phi_{2j+1}}{T\cos\phi_{2j+1}}u_{j+1} \\ &\quad + c(1+M_x)\nabla_y\cdot(v_{j+1}-v_j), \end{aligned} \tag{2.18}$$

$$\begin{aligned}(1+\cos\phi_{2j})\frac{\partial v_j}{\partial t} &= (1-\cos\phi_{2j+1})\frac{\partial v_{j+1}}{\partial t} - \frac{\sin^2\phi_{2j}}{T\cos\phi_{2j}}v_j - \frac{\sin^2\phi_{2j+1}}{T\cos\phi_{2j+1}}v_{j+1} \\ &\quad + c(1-M_x)\nabla_y(u_j-u_{j+1}), \end{aligned} \tag{2.19}$$

for $j=0,\cdots,P-1$. To close this system we use the fact that $\partial u_0/\partial x$ can be computed from the interior values and set

$$\frac{\partial u_0}{\partial t} = c(1-M_x)\frac{\partial u_0}{\partial x} + c\nabla_y\cdot v_0, \tag{2.20}$$

combined with the termination conditions

$$v_P = 0. \tag{2.21}$$

Eqs. (2.18)-(2.21), combined with the zero initial data and the boundary conditions on $\partial\Omega$, directly define the approximate boundary conditions. We can directly compute an expression for the reflection coefficient using (2.18)-(2.21); see [4] for details, as well as the analogous study of the linearized Euler equations below. As in [14] we express the reflection in terms of the data at $x=-L$. We then have the following result.

Theorem 2.1. *The solution of* (2.1) *terminated by* (2.18)-(2.21) *may be written*

$$\hat{u} = \sum_k \hat{u}_{k,+}(s)\psi_k(y)\left(e^{\lambda_{k,+}(x+L)} + \rho_k e^{\lambda_{k,-}(x+L)}\right), \quad x\in[-(L+\delta),-L],$$

where the reflection coefficient ρ_k is given by

$$\rho_k = e^{-\frac{2\delta}{1-M_x^2}\gamma_k}\left(\frac{\gamma_k-\bar{s}}{\gamma_k+\bar{s}}\right)\cdot\prod_{j=0}^{2P-1}\frac{\left(\gamma_k-\cos\phi_j\cdot\bar{s}-\frac{\sin^2\phi_j}{cT\cos\phi_j}\right)}{\left(\gamma_k+\cos\phi_j\cdot\bar{s}+\frac{\sin^2\phi_j}{cT\cos\phi_j}\right)}.$$

This reflection coefficient can be made uniformly smaller than ϵ on the contour $\Re\bar{s}=\frac{1}{cT}$ by choosing geometrically distributed cosines approximately on the interval $[\frac{2\delta}{(1-M_x^2)cT\ln 1/\epsilon},1]$. Precisely, by [14, Thm. 5.1],

$$P > C\cdot\ln\left(\frac{(1-M_x^2)cT}{\delta}\right)\cdot\ln\left(\frac{1}{\epsilon}\right) \tag{2.22}$$

suffices where C is universal constant. Direct computations of optimal cosines via the Remez algorithm reveal that C is not large. Note that as M_x increases somewhat fewer terms in the boundary condition are required.

2.1.2 Outflow boundary

The treatment of the outflow boundary, $x=L+\delta$ is similar, and in fact leads to exactly the same expression for the reflection coefficient. Now set

$$\frac{1-M_x}{c}\frac{\partial u}{\partial t}+\left(1-M_x^2\right)\frac{\partial u}{\partial x}=(1-M_x)\nabla_y\cdot v, \tag{2.23}$$

$$\frac{1+M_x}{c}\frac{\partial v}{\partial t}-\left(1-M_x^2\right)\frac{\partial v}{\partial x}=(1+M_x)\nabla_y u. \tag{2.24}$$

In contrast with the inflow case, u is now a right-moving normal characteristic variable while v is left-moving. We now have

$$\left(1-M_x^2\right)\frac{\partial q}{\partial x}=\mathcal{L}_O q, \tag{2.25}$$

and

$$\begin{aligned}&\mathcal{L}_O q_j-\frac{M_x-\cos\phi_{2j}}{c}\frac{\partial q_j}{\partial t}+\frac{\sin^2\phi_{2j}}{cT\cos\phi_{2j}}q_j\\ =&\mathcal{L}_O q_{j+1}-\frac{M_x+\cos\phi_{2j+1}}{c}\frac{\partial q_{j+1}}{\partial t}-\frac{\sin^2\phi_{2j+1}}{cT\cos\phi_{2j+1}}q_{j+1}.\end{aligned} \tag{2.26}$$

That is

$$\begin{aligned}\left(1+\cos\phi_{2j+1}\right)\frac{\partial u_{j+1}}{\partial t}=&\left(1-\cos\phi_{2j}\right)\frac{\partial u_j}{\partial t}-\frac{\sin^2\phi_{2j}}{T\cos\phi_{2j}}u_j-\frac{\sin^2\phi_{2j+1}}{T\cos\phi_{2j+1}}u_{j+1}\\ &+c(1-M_x)\nabla_y\cdot\left(v_{j+1}-v_j\right),\end{aligned} \tag{2.27}$$

$$\begin{aligned}\left(1+\cos\phi_{2j}\right)\frac{\partial v_j}{\partial t}=&\left(1-\cos\phi_{2j+1}\right)\frac{\partial v_{j+1}}{\partial t}-\frac{\sin^2\phi_{2j}}{T\cos\phi_{2j}}v_j-\frac{\sin^2\phi_{2j+1}}{T\cos\phi_{2j+1}}v_{j+1}\\ &+c(1+M_x)\nabla_y\left(u_j-u_{j+1}\right),\end{aligned} \tag{2.28}$$

for $j=0,\cdots,P-1$. To close this system we again compute $\partial u_0/\partial x$ from the interior values and set

$$\frac{\partial u_0}{\partial t}=-c(1+M_x)\frac{\partial u_0}{\partial x}+c\nabla_y\cdot v_0, \tag{2.29}$$

combined with the termination conditions

$$v_P=0. \tag{2.30}$$

As mentioned earlier, the reflection coefficients here are identical to those at inflow, and thus the requirements on P are still given by (2.22).

Theorem 2.2. *The solution of* (2.1) *terminated by* (2.27)-(2.30) *may be written*

$$\hat{u}=\sum_k \hat{u}_{k,-}(s)\psi_k(y)\left(e^{\lambda_{k,-}(x-L)}+\rho_k e^{\lambda_{k,+}(x-L)}\right),\quad x\in[L,L+\delta],$$

where the reflection coefficient ρ_k *is given by*

$$\rho_k=e^{-\frac{2\delta}{1-M_x^2}\gamma_k}\left(\frac{\gamma_k-s}{\gamma_k+s}\right)\cdot\prod_{j=0}^{2P-1}\frac{\left(\gamma_k-\cos\phi_j\cdot\bar{s}-\frac{\sin^2\phi_j}{cT\cos\phi_j}\right)}{\left(\gamma_k+\cos\phi_j\cdot\bar{s}+\frac{\sin^2\phi_j}{cT\cos\phi_j}\right)}.$$

2.2 Numerical experiments

To demonstrate the effectiveness of the proposed conditions we solve (2.1) for $0<t\leq 50$ with $d=1$ under the following conditions:

$$\Omega=(-1,1),\quad L=1,\quad \delta=.05,\quad c=1. \tag{2.31}$$

We take Dirichlet boundary conditions, that is $\alpha=0$ and $\beta=1$ in (2.2), zero initial data and

$$f(x,y,t)=300\sin(5\pi y)\cdot\sin^9(\pi x)\cdot\sin^9(2\pi t),\quad x\in[-1,1]. \tag{2.32}$$

We consider two cases, $M_x=.5$ and $M_x=.9$, and compare the errors in the numerical solutions for $P=5,9,13$. The cosine parameters, listed below in Table 1, are those obtained by minimizing the maximum of the reflection coefficient for $\frac{\delta}{cT}=10^{-3}$. This ignores the effect of $M_x>0$. A table of these coefficients, computed for various values of P and $\frac{\delta}{cT}$ using the Remez algorithm, is available at `http://faculty.smu.edu/thagstrom/rbcpac.html`. (Note that the definition of P in that table differs by one from the one given here.) The maximum reflection coefficients for these choices, again neglecting $M_x>0$, are 3.84×10^{-3}, 7.17×10^{-5}, and 1.57×10^{-6} respectively.

Our numerical method, described in more detail in [12], combines 8th order central differences in space with the standard 4th order Runge-Kutta method in time. The interior grid consists of a uniform grid with spacing h enhanced by a single layer of points near the boundaries, precisely at

$$x=\pm(1-.28h),\qquad y=\pm(1-.28h). \tag{2.33}$$

These additional points mitigate the Runge phenomenon and render the 8th order one-sided differencing at the boundary stable. To enable the use of the Runge-Kutta method (or any other standard explicit ode solver), we rewrite the system in first order form in time. For the approximate solution on the interior nodes we have

$$\frac{du_h}{dt}=-2M_xD_{1,x,h}u_h+\frac{1}{h}w_h, \tag{2.34}$$

$$\frac{dw_h}{dt}=h\left((1-M_x^2)D_{2,x,h}+D_{2,y,h}\right)u_h+V_hw_h+hf. \tag{2.35}$$

Table 1: Cosine parameters used in the numerical experiments: chosen to minimize the maximum of the reflection coefficient for $\frac{\delta}{cT}=10^{-3}$.

j	$P=5$	$P=9$	$P=13$
0	$6.040903414888e-01$	$8.084422182824e-01$	$8.893124828166e-01$
1	$2.944927016281e-01$	$5.659360392846e-01$	$7.200026603540e-01$
2	$1.358433303190e-01$	$3.682288161596e-01$	$5.475942643755e-01$
3	$6.191277943631e-02$	$2.321317430477e-01$	$4.014858028945e-01$
4	$2.814673833873e-02$	$1.444911730533e-01$	$2.885723502650e-01$
5	$1.278876043970e-02$	$8.949625706461e-02$	$2.052868351751e-01$
6	$5.808657972930e-03$	$5.532796448591e-02$	$1.452765225470e-01$
7	$2.635089551063e-03$	$3.417974749812e-02$	$1.025393146758e-01$
8	$1.188352578737e-03$	$2.110915237293e-02$	$7.227986833661e-02$
9	$5.189147034346e-04$	$1.303531760688e-02$	$5.091688915294e-02$
10		$8.048985222797e-03$	$3.585634377813e-02$
11		$4.969557269863e-03$	$2.524643972163e-02$
12		$3.067583851278e-03$	$1.777455749044e-02$
13		$1.892445141893e-03$	$1.251348547002e-02$
14		$1.165694094799e-03$	$8.809375553690e-03$
15		$7.150729419784e-04$	$6.201536203730e-03$
16		$4.335308401787e-04$	$4.365502591089e-03$
17		$2.527593467861e-04$	$3.072795296527e-03$
18			$2.162532543977e-03$
19			$1.521423107940e-03$
20			$1.069670264147e-03$
21			$7.510378539137e-04$
22			$5.258387432908e-04$
23			$3.659534016898e-04$
24			$2.511721752577e-04$
25			$1.658511245017e-04$

Here $D_{k,(x,y),h}$ denote 8th order difference approximations to the kth derivative in the x or y directions. Away from the boundaries these are simply the standard central difference operators. Near the boundaries they are simply defined by differentiating the Lagrange interpolants associated with the $k+8$ nearest nodes. The operator V_h provides 10th order dissipation in the interior, vanishing as one approaches the boundaries. For its precise definition and standard parameter choices, which we make here, see [12]. In this way it is not necessary to define w_h on the boundaries or provide boundary conditions for it. The time derivative of u_h at $y=\pm 1$ is zero, while at $x=\pm 1$ it is given by discretizations of (2.20) and (2.29) using the one-sided difference approximations in x, and also in y for nodes near the top and bottom. The recursions (2.18), (2.19), (2.27) and (2.28), combined with the difference operator $D_{1,y,h}$, provide the remaining time derivatives. For the experiments below we choose $h=10^{-2}$ and $\Delta t=10^{-3}$. Approximate error data is obtained by comparison with solutions computed using the same values of h and Δt but on a large

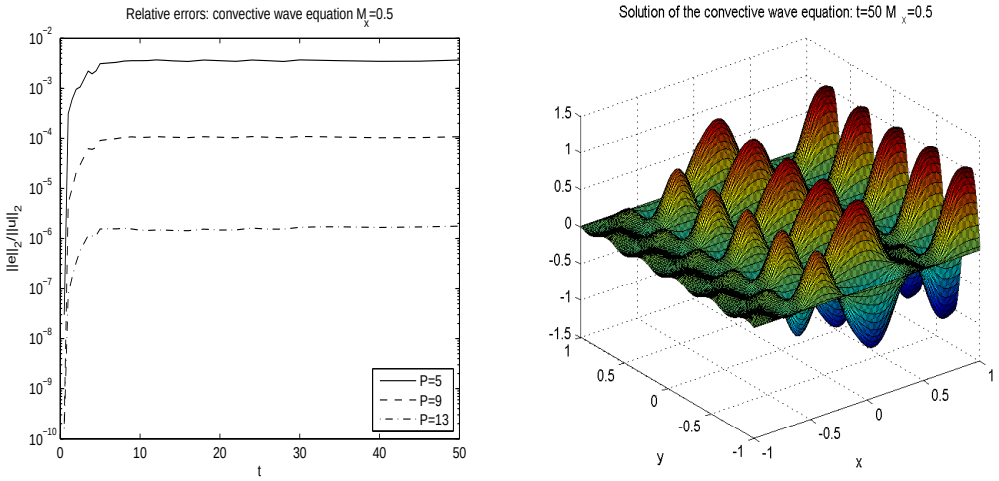

Figure 1: Results for the convective wave equation with $M_x = 0.5$.

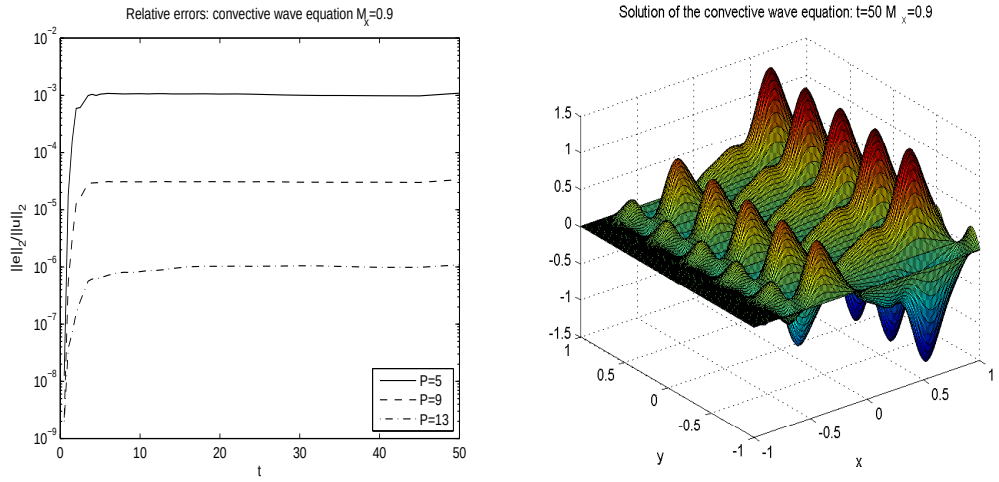

Figure 2: Results for the convective wave equation with $M_x = 0.9$.

domain, $(-26,26)\times(-1,1)$. Here reflections from the artificial boundaries cannot reach into the interior by $t = 50$.

In Fig. 1 we display the relative L^2-errors computed at various times and for the three values of P and $M_x = 0.5$. We note that after an initial transient phase the errors saturate, displaying no visible growth over time. The error levels themselves are commensurate with the maximum values of the reflection coefficients. We also plot the solution itself at $t = 50$.

In Fig. 2 we display the relative L^2-errors computed at various times and for the three values of P and $M_x = 0.9$. The results are quite similar to those obtained for $M_x = 0.5$, though with slightly reduced error levels. This is consistent with the M_x-dependence of

the reflection coefficients in Theorem 2.1 and Theorem 2.2. The solution at $t=50$ is also displayed.

3 The linearized Euler equations

We now consider the isentropic compressible Euler equations linearized about a uniform subsonic flow,

$$\frac{\partial p}{\partial t}+V_x\frac{\partial p}{\partial x}+\bar{\rho}c^2\nabla\cdot v=f_p, \tag{3.1a}$$

$$\frac{\partial v}{\partial t}+V_x\frac{\partial v}{\partial x}+\bar{\rho}^{-1}\nabla p=f_v, \tag{3.1b}$$

where p is the pressure and $v=(u,v_y)^T$ is the velocity vector. Again we assume (2.3) and, the duct geometry

$$(x,y)\in\mathbb{R}\times\Omega, \qquad v_y\cdot n=0, \qquad y\in\partial\Omega, \tag{3.2}$$

with $p(x,y,0)$, $v(x,y,0)$, $f_p(x,y,t)$, and $f_v(x,y,t)$ supported in $(-L,L)\times\Omega$.

It is easily seen that the pressure, p, satisfies the convective wave equation (2.1) and a Neumann boundary condition on $\partial\Omega$. This governs the evolution of the sound waves. However, the linearized Euler equations support, in addition, vorticity modes. We will see that their presence requires some modification of the boundary recursions, both to guarantee stability and to provide accuracy.

3.1 Construction and analysis of the boundary conditions

As in the case of the convective wave equation we compute modal solutions in the tails following a Laplace transformation in time. To simplify the calculations we first rewrite the system by introducing the normal characteristic variables and scaling the velocities

$$l=p-\bar{\rho}cu, \qquad r=p+\bar{\rho}cu, \qquad w=\bar{\rho}cv_y, \tag{3.3}$$

and set $q=(l \quad r \quad w)^T$. Anticipating their use to eliminate normal derivatives from the boundary recursions we note that q satisfies

$$\left(1-M_x^2\right)q_x=\begin{pmatrix} \frac{(1+M_x)}{c}\left(\frac{\partial l}{\partial t}+c\nabla_y\cdot w\right) \\ -\frac{(1-M_x)}{c}\left(\frac{\partial r}{\partial t}+c\nabla_y\cdot w\right) \\ -\frac{\left(1-M_x^2\right)}{cM_x}\left(\frac{\partial w}{\partial t}+\frac{c}{2}\nabla_y(l+r)\right)\end{pmatrix}\equiv\mathcal{G}q. \tag{3.4}$$

As the acoustic modes are governed by the convective wave equation, we define $\lambda_{k,\pm}$ via (2.8)-(2.9) and set $\psi_k(y)$ to be a Neumann eigenfunction of the Laplacian in Ω. For a

leftgoing mode set $\hat{l}=\psi_k$. Clearly, by (3.4) we must have $\hat{r}\propto\psi_k$ and $\hat{w}\propto\nabla_y\psi_k$. Making use of the identity

$$\nabla_y^2\psi_k=-\eta_k^2\psi_k=-\frac{(\gamma_k-\bar{s})(\gamma_k+\bar{s})}{(1-M_x^2)}, \tag{3.5}$$

we find

$$\hat{q}_{k,+}=e^{\lambda_{k,+}x}\begin{pmatrix}\psi_k\\ -\frac{(1-M_x)}{(1+M_x)}\frac{\gamma_k-\bar{s}}{\gamma_k+\bar{s}}\psi_k\\ -\frac{(1-M_x)}{\gamma_k+\bar{s}}\nabla_y\psi_k\end{pmatrix}\equiv e^{\lambda_{k,+}x}\bar{q}_{k,+}. \tag{3.6}$$

Similarly we compute the rightgoing mode

$$\hat{q}_{k,-}=e^{\lambda_{k,-}x}\begin{pmatrix}-\frac{(1+M_x)}{(1-M_x)}\frac{\gamma_k-\bar{s}}{\gamma_k+\bar{s}}\psi_k\\ \psi_k\\ -\frac{(1+M_x)}{\gamma_k+\bar{s}}\nabla_y\psi_k\end{pmatrix}\equiv e^{\lambda_{k,-}x}\bar{q}_{k,-}. \tag{3.7}$$

The vorticity modes are rightmoving and correspond to

$$\lambda_0=-\frac{\bar{s}}{M_x}. \tag{3.8}$$

They are given by

$$\hat{\omega}=e^{\lambda_0 x}\begin{pmatrix}-\frac{M_x}{\bar{s}}\nabla_y\cdot\Upsilon\\ -\frac{M_x}{\bar{s}}\nabla_y\cdot\Upsilon\\ \Upsilon\end{pmatrix}\equiv e^{\lambda_0 x}\bar{\omega}, \tag{3.9}$$

where $\Upsilon(y)$ is any function satisfying $\Upsilon\cdot n=0$ on $\partial\Omega$.

Exact nonlocal conditions for the linearized Euler equations, analogous to (2.10) and (2.11) have been devised and implemented [1, 2, 10]. A complicating fact, noticed first by Giles [8], is that certain natural exact formulations at inflow are not well-posed due to the coincidence of $\lambda_{k,-}$ and λ_0 for special values of $\bar{s}$.

For our formulation, we will exclude this possibility by modifying the boundary recursions not only at outflow, where the additional vorticity mode must be absorbed, but also at inflow, where it can be generated.

3.1.1 Inflow boundary

At the inflow boundary we require two boundary conditions corresponding to the two rightgoing modes. Introducing angles ϕ_j, $j=0,\cdots,2P$ we formally write down recursions starting from $q_0\equiv q$, analogous to (2.17). The exception is the first term, where an operator annihilating vorticity modes,

$$\mathcal{G}+\frac{1-M_x^2}{cM_x}\frac{\partial}{\partial t} \tag{3.10}$$

is applied to q_1. We thus derive the equations for computing the evolution of the auxiliary variables on the boundary.

$$\left(\frac{1+M_x}{M_x}\right)\frac{\partial l_1}{\partial t}=(1-\cos\phi_0)\frac{\partial l_0}{\partial t}-\frac{\sin^2\phi_0}{T\cos\phi_0}l_0+c(1+M_x)\nabla_y\cdot(w_0-w_1), \tag{3.11}$$

$$(1+\cos\phi_0)\frac{\partial r_0}{\partial t}=-\left(\frac{1-M_x}{M_x}\right)\frac{\partial r_1}{\partial t}-\frac{\sin^2\phi_0}{T\cos\phi_0}r_0+c(1-M_x)\nabla_y\cdot(w_1-w_0), \tag{3.12}$$

$$(1+M_x\cos\phi_0)\frac{\partial w_0}{\partial t}=-\frac{M_x\sin^2\phi_0}{T\cos\phi_0}w_0+\frac{c}{2}\left(1-M_x^2\right)\nabla_y(l_1+r_1-l_0-r_0), \tag{3.13}$$

$$\begin{aligned}\left(1+\cos\phi_{2j}\right)\frac{\partial l_{j+1}}{\partial t}=&\left(1-\cos\phi_{2j-1}\right)\frac{\partial l_j}{\partial t}-\frac{\sin^2\phi_{2j-1}}{T\cos\phi_{2j-1}}l_j-\frac{\sin^2\phi_{2j}}{T\cos\phi_{2j}}l_{j+1}\\&+c(1+M_x)\nabla_y\cdot\left(w_j-w_{j+1}\right),\end{aligned} \tag{3.14}$$

$$\begin{aligned}\left(1+\cos\phi_{2j-1}\right)\frac{\partial r_j}{\partial t}=&\left(1-\cos\phi_{2j}\right)\frac{\partial r_{j+1}}{\partial t}-\frac{\sin^2\phi_{2j-1}}{T\cos\phi_{2j-1}}r_j-\frac{\sin^2\phi_{2j}}{T\cos\phi_{2j}}r_{j+1}\\&+c(1-M_x)\nabla_y\cdot\left(w_{j+1}-w_j\right),\end{aligned} \tag{3.15}$$

$$\begin{aligned}\left(1+M_x\cos\phi_{2j-1}\right)\frac{\partial w_j}{\partial t}=&\left(1-M_x\cos\phi_{2j}\right)\frac{\partial w_{j+1}}{\partial t}-\frac{M_x\sin^2\phi_{2j-1}}{T\cos\phi_{2j-1}}w_j-\frac{M_x\sin^2\phi_{2j}}{T\cos\phi_{2j}}w_{j+1}\\&+\frac{c}{2}\left(1-M_x^2\right)\nabla_y\left(l_{j+1}+r_{j+1}-l_j-r_j\right).\end{aligned} \tag{3.16}$$

As above, we close the system by computing $\partial l_0/\partial t$ using one-sided differencing

$$\frac{\partial l_0}{\partial t}=(c-V_x)\frac{\partial l_0}{\partial x}-c\nabla_y\cdot w \tag{3.17}$$

and imposing termination conditions

$$r_{P+1}=0,\quad w_{P+1}=0. \tag{3.18}$$

To estimate the reflection coefficients we expand the auxiliary functions using $\bar{q}_{k,\pm}$ from (3.6),(3.7) and $\bar{\omega}$ from (3.9). Due to the structure of the recursions, the coefficients in these expansions decouple. The vectors $\bar{q}_{k,\pm}$ and $\bar{\omega}$ are eigenvectors of $\mathcal{G}(s,\nabla_y)$ with eigenvalues $(1-M_x^2)\lambda_{k,\pm}$ and $(1-M_x^2)\lambda_0$. Writing

$$\hat{q}_j=\sum_k L_{k,j}\hat{q}_{k,+}+\sum_k R_{k,j}\hat{q}_{k,-}+\bar{\omega}_j, \tag{3.19}$$

we deduce

$$\left((\gamma_k-\cos\phi_0\bar{s})-\frac{\sin^2\phi_0}{cT\cos\phi_0}\right)L_{k,0}=\left(\frac{\bar{s}+M_x\gamma_k}{M_x}\right)L_{k,1}, \tag{3.20a}$$

$$\left((\gamma_k-\cos\phi_{2j-1}\bar{s})-\frac{\sin^2\phi_{2j-1}}{cT\cos\phi_{2j-1}}\right)L_{k,j}=\left((\gamma_k+\cos\phi_{2j}\bar{s})+\frac{\sin^2\phi_{2j}}{cT\cos\phi_{2j}}\right)L_{k,j+1}, \tag{3.20b}$$

which implies

$$L_{k,P+1}=\frac{M_x\left((\gamma_k-\cos\phi_0\bar{s})-\frac{\sin^2\phi_0}{cT\cos\phi_0}\right)}{\bar{s}+M_x\gamma_k}\prod_{j=1}^{P}\frac{\left((\gamma_k-\cos\phi_{2j-1}\bar{s})-\frac{\sin^2\phi_{2j-1}}{cT\cos\phi_{2j-1}}\right)}{\left((\gamma_k+\cos\phi_{2j}\bar{s})+\frac{\sin^2\phi_{2j}}{cT\cos\phi_{2j}}\right)}L_{k,0}, \tag{3.21}$$

and

$$\left((\gamma_k+\cos\phi_0\bar{s})+\frac{\sin^2\phi_0}{cT\cos\phi_0}\right)R_{k,0}=\left(\frac{-\bar{s}+M_x\gamma_k}{M_x}\right)R_{k,1}, \tag{3.22a}$$

$$\left((\gamma_k+\cos\phi_{2j-1}\bar{s})+\frac{\sin^2\phi_{2j-1}}{cT\cos\phi_{2j-1}}\right)R_{k,j}=\left((\gamma_k-\cos\phi_{2j}\bar{s})-\frac{\sin^2\phi_{2j}}{cT\cos\phi_{2j}}\right)R_{k,j+1}, \tag{3.22b}$$

which implies

$$R_{k,0}=\frac{-\bar{s}+M_x\gamma_k}{M_x\left((\gamma_k+\cos\phi_0\bar{s})+\frac{\sin^2\phi_0}{cT\cos\phi_0}\right)}\prod_{j=1}^{P}\frac{\left((\gamma_k-\cos\phi_{2j}\bar{s})-\frac{\sin^2\phi_{2j}}{cT\cos\phi_{2j}}\right)}{\left((\gamma_k+\cos\phi_{2j-1})\,\bar{s}+\frac{\sin^2\phi_{2j-1}}{cT\cos\phi_{2j-1}}\right)}R_{k,P+1}, \tag{3.23}$$

and finally

$$\left(\frac{(1+M_x\cos\phi_0)}{M_x}\bar{s}+\frac{\sin^2\phi_0}{cT\cos\phi_0}\right)\bar{\omega}_0=0 \tag{3.24}$$

which implies

$$\bar{\omega}_0=0. \tag{3.25}$$

That is, incoming vorticity modes cannot exist.

We now impose the termination conditions (3.18). Since $w_{P+1}=0$

$$\bar{\omega}_{P+1}=\begin{pmatrix} -\frac{M_x}{\bar{s}}\nabla_y\cdot W_{p+1}(y) \\ \frac{M_x}{\bar{s}}\nabla_y\cdot W_{p+1}(y) \\ W_{P+1}(y)\end{pmatrix}, \tag{3.26}$$

where

$$W_{P+1}(y)=\sum_k\frac{1}{\gamma_k+\bar{s}}((1-M_x)L_{k,P+1}+(1+M_x)R_{k,P+1})\nabla_y\psi_k(y). \tag{3.27}$$

Thus, recalling (3.5), the condition $r_{P+1}=0$ reduces to

$$-\frac{M_x(\gamma_k-\bar{s})}{(1-M_x^2)\bar{s}}((1-M_x)L_{k,P+1}+(1+M_x)R_{k,P+1})-\frac{1-M_x}{1+M_x}\frac{\gamma_k-\bar{s}}{\gamma_k+\bar{s}}L_{k,P+1}+R_{k,P+1}=0. \tag{3.28}$$

This implies

$$R_{k,P+1}=\left(\frac{1-M_x}{1+M_x}\right)\left(\frac{\bar{s}+M_x\gamma_k}{\bar{s}-M_x\gamma_k}\right)\left(\frac{\gamma_k-\bar{s}}{\gamma_k+\bar{s}}\right)L_{k,P+1}. \tag{3.29}$$

Combining (3.21),(3.23),(3.25), and (3.29) we have proven the following Theorem. Note that by (2.22) we can make the reflection small using only a few terms.

Theorem 3.1. *The solution of* (3.1) *terminated by* (3.11)-(3.18) *may be written*

$$\hat{q}=\sum_k \hat{\mu}_{k,+}(s)\left(e^{\lambda_{k,+}(x+L)}\bar{q}_{k,+}+\rho_k e^{\lambda_{k,-}(x+L)}\bar{q}_{k,-}\right),\quad x\in[-(L+\delta),-L],$$

where the reflection coefficient ρ_k *is given by*

$$\rho_k=-e^{-\frac{2\delta}{1-M_x^2}\gamma_k}\left(\frac{1-M_x}{1+M_x}\right)\left(\frac{\gamma_k-\bar{s}}{\gamma_k+\bar{s}}\right)\cdot\prod_{j=0}^{2P}\frac{\left(\gamma_k-\cos\phi_j\cdot\bar{s}-\frac{\sin^2\phi_j}{cT\cos\phi_j}\right)}{\left(\gamma_k+\cos\phi_j\cdot\bar{s}+\frac{\sin^2\phi_j}{cT\cos\phi_j}\right)}.$$

3.1.2 Outflow boundary

Our treatment of the outflow boundary is analogous to the case described above. A difference is that we must treat a vorticity mode impinging on the boundary rather than reflecting from it. Therefore the special operator (3.10) included to annihilate such modes appears on the lefthand side of the recursion rather than on the right, and the placement of the approximations to $\lambda_{k,\pm}$ are similarly reversed. We thus solve

$$\left(\frac{1+M_x}{M_x}\right)\frac{\partial l_0}{\partial t}=(1-\cos\phi_0)\frac{\partial l_1}{\partial t}-\frac{\sin^2\phi_0}{T\cos\phi_0}l_1+c(1+M_x)\nabla_y\cdot(w_1-w_0),\tag{3.30}$$

$$(1+\cos\phi_0)\frac{\partial r_1}{\partial t}=-\left(\frac{1-M_x}{M_x}\right)\frac{\partial r_0}{\partial t}-\frac{\sin^2\phi_0}{T\cos\phi_0}r_1+c(1-M_x)\nabla_y\cdot(w_0-w_1),\tag{3.31}$$

$$(1+M_x\cos\phi_0)\frac{\partial w_1}{\partial t}=-\frac{M_x\sin^2\phi_0}{T\cos\phi_0}w_0+\frac{c}{2}(1-M_x^2)\nabla_y(l_0+r_0-l_1-r_1),\tag{3.32}$$

$$\begin{aligned}(1+\cos\phi_{2j-1})\frac{\partial l_j}{\partial t}=(1-\cos\phi_{2j})\frac{\partial l_{j+1}}{\partial t}&-\frac{\sin^2\phi_{2j-1}}{T\cos\phi_{2j-1}}l_j-\frac{\sin^2\phi_{2j}}{T\cos\phi_{2j}}l_{j+1}\\&+c(1+M_x)\nabla_y\cdot(w_{j+1}-w_j),\end{aligned}\tag{3.33}$$

$$\begin{aligned}(1+\cos\phi_{2j})\frac{\partial r_{j+1}}{\partial t}=(1-\cos\phi_{2j-1})\frac{\partial r_j}{\partial t}&-\frac{\sin^2\phi_{2j-1}}{T\cos\phi_{2j-1}}r_j-\frac{\sin^2\phi_{2j}}{T\cos\phi_{2j}}r_{j+1}\\&+c(1-M_x)\nabla_y\cdot(w_j-w_{j+1}),\end{aligned}\tag{3.34}$$

$$\begin{aligned}(1+M_x\cos\phi_{2j})\frac{\partial w_{j+1}}{\partial t}=(1-M_x\cos\phi_{2j-1})\frac{\partial w_j}{\partial t}&-\frac{M_x\sin^2\phi_{2j-1}}{T\cos\phi_{2j-1}}w_j-\frac{M_x\sin^2\phi_{2j}}{T\cos\phi_{2j}}w_{j+1}\\&+\frac{c}{2}(1-M_x^2)\nabla_y(l_j+r_j-l_{j+1}-r_{j+1}).\end{aligned}\tag{3.35}$$

Now there are two modes computed from the interior

$$\frac{\partial r_0}{\partial t}=-(c+V_x)\frac{\partial r_0}{\partial x}-c\nabla_y\cdot w_0,\tag{3.36}$$

$$\frac{\partial w_0}{\partial t}=-V_x\frac{\partial w_0}{\partial x}-\frac{c}{2}\nabla_y(l_0+r_0),\tag{3.37}$$

and a single termination condition

$$l_{P+1}=0. \tag{3.38}$$

We compute the reflection coefficient as in the inflow case:

$$\left(\frac{\bar{s}+M_x\gamma_k}{M_x}\right)L_{k,0}=\left((\gamma_k-\cos\phi_0\bar{s})-\frac{\sin^2\phi_0}{cT\cos\phi_0}\right)L_{k,1}, \tag{3.39a}$$

$$\left((\gamma_k+\cos\phi_{2j-1}\bar{s})+\frac{\sin^2\phi_{2j-1}}{cT\cos\phi_{2j-1}}\right)L_{k,j}=\left((\gamma_k-\cos\phi_{2j}\bar{s})-\frac{\sin^2\phi_{2j}}{cT\cos\phi_{2j}}\right)L_{k,j+1}, \tag{3.39b}$$

which implies

$$L_{k,0}=\frac{M_x\left((\gamma_k-\cos\phi_0\bar{s})-\frac{\sin^2\phi_0}{cT\cos\phi_0}\right)}{\bar{s}+M_x\gamma_k}\prod_{j=1}^{P}\frac{\left((\gamma_k-\cos\phi_{2j}\bar{s})-\frac{\sin^2\phi_{2j}}{cT\cos\phi_{2j}}\right)}{\left((\gamma_k+\cos\phi_{2j-1}\bar{s})+\frac{\sin^2\phi_{2j-1}}{cT\cos\phi_{2j-1}}\right)}L_{k,P+1}, \tag{3.40}$$

and

$$\left(\frac{-\bar{s}+M_x\gamma_k}{M_x}\right)R_{k,0}=\left((\gamma_k+\cos\phi_0)\bar{s}+\frac{\sin^2\phi_0}{cT\cos\phi_0}\right)R_{k,1}, \tag{3.41a}$$

$$\left((\gamma_k-\cos\phi_{2j-1}\bar{s})-\frac{\sin^2\phi_{2j-1}}{cT\cos\phi_{2j-1}}\right)R_{k,j}=\left((\gamma_k+\cos\phi_{2j}\bar{s})+\frac{\sin^2\phi_{2j}}{cT\cos\phi_{2j}}\right)R_{k,j+1}, \tag{3.41b}$$

which implies

$$R_{k,P+1}=\frac{-\bar{s}+M_x\gamma_k}{M_x\left((\gamma_k+\cos\phi_0\bar{s})+\frac{\sin^2\phi_0}{cT\cos\phi_0}\right)}\prod_{j=1}^{P}\frac{\left((\gamma_k-\cos\phi_{2j-1}\bar{s})-\frac{\sin^2\phi_{2j-1}}{cT\cos\phi_{2j-1}}\right)}{\left((\gamma_k+\cos\phi_{2j})\bar{s}+\frac{\sin^2\phi_{2j}}{cT\cos\phi_{2j}}\right)}R_{k,0}, \tag{3.42}$$

and finally

$$\left(\frac{(1+M_x\cos\phi_0)}{M_x}\bar{s}+\frac{\sin^2\phi_0}{cT\cos\phi_0}\right)\bar{\omega}_1=0, \tag{3.43a}$$

$$\left((1-M_x\cos\phi_{2j-1}\bar{s})-\frac{M_x\sin^2\phi_{2j-1}}{cT\cos\phi_{2j-1}}\right)\bar{\omega}_j=\left((1+M_x\cos\phi_{2j}\bar{s})+\frac{M_x\sin^2\phi_{2j}}{cT\cos\phi_{2j}}\right)\bar{\omega}_{j+1}, \tag{3.43b}$$

which implies

$$\bar{\omega}_j=0,\quad j>0. \tag{3.44}$$

Lastly we impose (3.38) which due to (3.44) implies

$$L_{k,P+1}=\left(\frac{1+M_x}{1-M_x}\right)\left(\frac{\gamma_k-\bar{s}}{\gamma_k+\bar{s}}\right)R_{k,P+1}. \tag{3.45}$$

Combining (3.40), (3.42), (3.44), and (3.45) we have proven the following theorem. Again by (2.22) we can make the reflection small using only a few terms.

Theorem 3.2. *The solution of* (3.1) *terminated by* (3.30)-(3.38) *may be written*

$$\hat{q}=\sum_k \hat{v}_{k,-}(s)\left(e^{\lambda_{k,-}(x-L)}\bar{q}_{k,-}+\rho_k e^{\lambda_{k,+}(x-L)}\bar{q}_{k,+}\right)+\hat{\zeta}(s)e^{\lambda_0(x-L)}\bar{\omega},\quad x\in[L,L+\delta],$$

where the reflection coefficient ρ_k *is given by*

$$\rho_k=-e^{-\frac{2\delta}{1-M_x^2}\gamma_k}\left(\frac{1+M_x}{1-M_x}\right)\left(\frac{\bar{s}-M_x\gamma_k}{\bar{s}+M_x\gamma_k}\right)\left(\frac{\gamma_k-\bar{s}}{\gamma_k+\bar{s}}\right)\cdot\prod_{j=0}^{2P}\frac{\left(\gamma_k-\cos\phi_j\cdot\bar{s}-\frac{\sin^2\phi_j}{cT\cos\phi_j}\right)}{\left(\gamma_k+\cos\phi_j\cdot\bar{s}+\frac{\sin^2\phi_j}{cT\cos\phi_j}\right)}.$$

3.2 Numerical experiments

We have also carried out numerical experiments for the linearized Euler equations similar to those reported above for the convective wave equation. We solve (3.1) for $0<t\leq 50$ with $d=1$ under the following conditions:

$$\Omega=(-1,1),\quad L=1,\quad \delta=.05,\quad c=1,\quad \bar{\rho}=1. \tag{3.46}$$

We take zero initial data, $f_p=0$ and $f_v(x,y,t)=(f_x(x,y,t),f_y(x,y,t))^T$ supported in $x\in[-1,1]$ given by

$$\begin{aligned} f_x(x,y,t)&=10\cos(5\pi y)\cdot\sin^{10}(\pi x)\cdot\sin^9(2\pi t),\\ f_y(x,y,t)&=10\sin(5\pi y)\cdot\sin^{10}(\pi x)\cdot\sin^9(2\pi t). \end{aligned} \tag{3.47}$$

Notice that f is neither solenoidal nor irrotational, so both acoustic and vortical modes will be excited.

Again we consider the two cases, $M_x=.5$ and $M_x=.9$, and compare the errors in the numerical solutions for $P=5,9,13$. Notice that we require one more cosine value than for the comparable cases with the convective wave equation. We choose the cosines to be the same as for these previous experiments with the additional angle $\phi=0$. Note that the ordering of the parameters has no effect on the reflection coefficient, and in our experiments we set $\phi_0=0$ so that ϕ_j here corresponds to ϕ_{j-1} from above.

As before our numerical method combines 8th order central differences in space with the standard 4th order Runge-Kutta method in time. The interior grid consists of a uniform grid with spacing h enhanced by a single layer of points near the boundaries, now at

$$x=\pm(1-.2h),\qquad y=\pm(1-.2h), \tag{3.48}$$

as advocated for first-order systems in [11]. As all time derivatives are already first order, no additional variables are needed to enable the use of the Runge-Kutta method. Also,

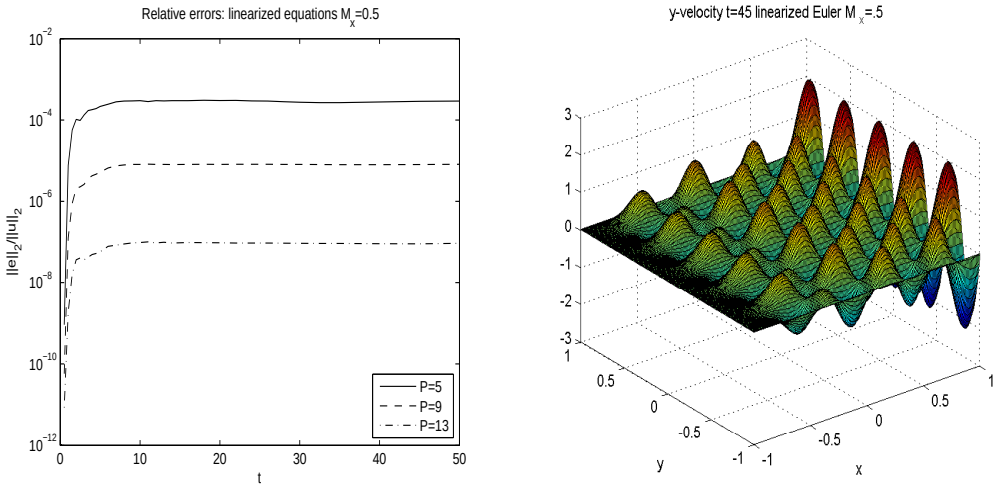

Figure 3: Results for the linearized Euler equations with $M_x = 0.5$.

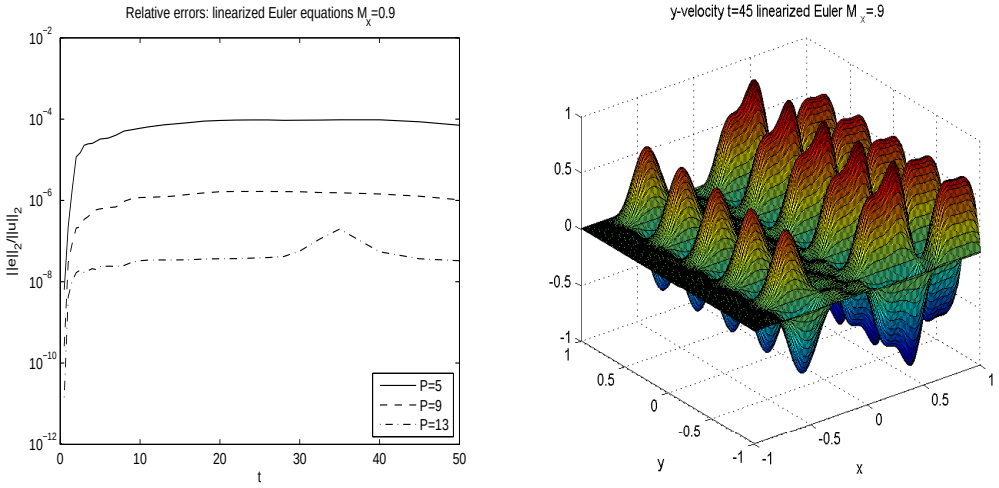

Figure 4: Results for the linearized Euler equations with $M_x = 0.9$.

in this case, we did not include a dissipation operator. The mesh spacing, $h = 10^{-2}$, time step, $\Delta t = 10^{-3}$, and method for generating error data are identical to those used in the earlier experiments.

In Fig. 3 we display the relative L^2-errors computed at various times and for the three values of P and $M_x = 0.5$. We note that after an initial transient phase the errors saturate, displaying no visible growth over time. The error levels themselves are somewhat smaller than for the convective wave equation, which could be explained by the presence of an additional term in the boundary conditions and the fact that the vorticity modes are treated exactly. The y-velocity field at $t = 45$ is also plotted.

In Fig. 4 we display the relative L^2-errors computed at various times and for the three

values of P and $M_x = 0.9$. The results are quite similar to those obtained for $M_x = 0.5$, though again with slightly reduced error levels for $P = 5$ and $P = 9$. The errors in the case $P = 13$ exhibit a peak of about 2×10^{-7} at $t = 35$. We do not have a clear explanation for this peak, but plots of the error suggest it is primarily due to the discretization, not the boundary treatment. The y-velocity at $t = 45$ is also displayed.

4 Conclusions

We have demonstrated, both theoretically and practically, that high-order radiation boundary conditions based on the so-called complete wave representation provide outstanding accuracy at negligible cost. We note that they can also be applied to the more general anisotropic systems considered in [4], and can be applied in exterior geometries using corner compatibility conditions, as developed for isotropic problems in [14]. The fundamental open issue is their generalization to anisotropic systems, such as those arising in the study of elastic waves in crystals [3].

Acknowledgments

The first and fourth authors were supported in part by ARO Grant W911NF-09-1-0344. The first and third authors were supported in part by BSF grant 2008096. The first author was also supported in part by NSF grant OCI-0904773. Any conclusions or recommendations expressed in this paper are those of the authors and do not necessarily reflect the views of NSF, ARO, or BSF.

References

[1] O. Atassi. Nonreflecting boundary conditions for the time-dependent convective wave equation in a duct. J. Comput. Phys., 197:737–758, 2004.
[2] O. Atassi and J. Galán. Implementation of nonreflecting boundary conditions for the nonlinear Euler equations. J. Comput. Phys., 227:1643–1662, 2008.
[3] E. Bécache, S. Fauqueux, and P. Joly. Stability of perfectly matched layers, group velocities, and anisotropic waves. J. Comput. Phys., 188:399–433, 2003.
[4] E. Bécache, D. Givoli, and T. Hagstrom. High-order Absorbing Boundary Conditions for anisotropic and convective wave equations. J. Comput. Phys., 229:1099–1129, 2010.
[5] A. Bayliss and E. Turkel. Far field boundary conditions for compressible flows. J. Comput. Phys., 48:182–199, 1982.
[6] J. Diaz and P. Joly. Stabilized perfectly matched layer for advective acoustics. In G. Cohen, E. Heikkola, P. Joly, and P. Neittaanmäki, editors, Mathematical and Numerical Aspects of Wave Propagation Phenomena, pages 115–119. Springer, 2003.
[7] J. Diaz and P. Joly. A time-domain analysis of PML models in acoustics. Computer Meth. Appl. Mech. Engrg., 195:3820–3853, 2006.
[8] M. Giles. Nonreflecting boundary conditions for Euler equation calculations. AIAA J., 28:2050–2058, 1990.

[9] T. Hagstrom. A new construction of perfectly matched layers for hyperbolic systems with applications to the linearized Euler equations. In G. Cohen, E. Heikkola, P. Joly, and P. Neittaanmäki, editors, Mathematical and Numerical Aspects of Wave Propagation Phenomena, pages 125–129. Springer, 2003.
[10] T. Hagstrom and J. Goodrich. Accurate radiation boundary conditions for the linearized Euler equations in Cartesian domains. SIAM J. Sci. Comput., 24:770–795, 2002.
[11] T. Hagstrom and G. Hagstrom. Grid stabilization of high-order one-sided differencing I: First order hyperbolic systems. J. Comput. Phys., 223:316–340, 2007.
[12] T. Hagstrom and G. Hagstrom. Grid stabilization of high-order one-sided differencing II: Second order wave equations. Submitted, 2009.
[13] T. Hagstrom, S.I. Hariharan, and D. Thompson. High-order radiation boundary conditions the convective wave equation in exterior domains. SIAM J. Sci. Comput., 25:1088–1101, 2003.
[14] T. Hagstrom and T. Warburton. Complete radiation boundary conditions: Minimizing the long time error growth of local methods. SIAM J. Numer. Anal., 47:3678–3704, 2009.
[15] F. Hu. A stable, perfectly matched layer for linearized Euler equations in unsplit physical variables. J. Comput. Phys., 173:455–480, 2001.
[16] D. Rudy and J. Strikwerda. A nonreflecting outflow boundary condition for subsonic Navier-Stokes calculations. J. Comput. Phys., pages 55–70, 1980.